polysaccharides

MDPI

Article

Extraction-Induced Molecular Balance Governs the Film-Forming and Emulsion-Stabilizing Performance of Yellow Passion-Fruit-Peel Mucilage Pectins

Nivea Mabel, Mayana Morais de Sousa, Sibelly Barbosa, Shenia Santos Monteiro, Thaisa Abrantes Souza Gusmão, Hugo M. Lisboa * and Matheus Augusto Bittencourt Pasquali *

Food Engineering Department, Federal University of Campina Grande, Campina Grande 58429-900, Paraiba, Brazil; thaisa.abrantes@professor.udcf.edu.br (T.A.S.G.)

* Correspondence: hugo.miguel@professor.ufcg.edu.br (H.M.L.); matheus.augusto@professor.ufcg.edu.br (M.A.B.P.)

Abstract

Five pectin-rich mucilage fractions from yellow passion-fruit peel, extracted using 0–10.0% (*w*/*v*) citric acid, were evaluated in separate films and sunflower-oil emulsions. The 0.086% fraction gave the highest mean tensile strength and Young's modulus (31.26 and 468.9 MPa), while 0.086–0.50% produced the lowest water-vapor permeability (1.70–1.82 × 10^{-10} g m m^{-2} s^{-1} Pa^{-1}). The 0.50% fraction produced the smallest initial and day 21 emulsion droplets (1.72 and 1.81 µm) and the lowest day 21 creaming (2.0%). At 10.0% acid, film strength decreased to 3.34 MPa, while emulsion droplets reached 5.31 µm and creaming reached 28.1%, despite the most negative ζ-potential (−56.0 mV). These responses are consistent with reduced molecular integrity under severe extraction and indicate that charge alone does not determine performance. Under the tested formulations, mild extraction at 0.086–0.50% citric acid provided the most favorable combination of film and emulsion properties.

Keywords: passion fruit peel; pectin; citric acid extraction; pectin films; emulsion stability; structure–function relationships

1. Introduction

Yellow passion-fruit processing generates a peel-rich by-product that contains substantial amounts of pectic polysaccharides. Recovering pectin from this material can reduce disposal burdens and create a food-grade hydrocolloid source, but the usefulness of the recovered material depends on more than gravimetric yield [1]. Pectin is a heterogeneous macromolecular family containing homogalacturonan-rich regions and rhamnogalacturonan-I domains with arabinan, galactan, and arabinogalactan substituents. Its degree and pattern of methyl esterification, chain size, branching, charge density, associated protein, and conformation collectively determine hydration, rheology, gelation, interfacial behavior, and film formation [2].

Citric acid is attractive for food-compatible pectin extraction, yet concentration and thermal history can shift the process from selective solubilization to de-esterification, debranching, and backbone cleavage [3,4]. Previous work on passion-fruit peel has shown that extraction route changes GalA content, molar mass, esterification, rheology, and emulsion stability [5–7]. A selected citric acid severity series is therefore useful not only

Check for updates

Academic Editor: Cédric Delattre

Received: 28 August 2026
Revised: 23 September 2026
Accepted: 24 September 2026
Published: 29 September 2026

Copyright: © 2026 by the authors. Licensee MDPI, Basel, Switzerland. This article is an open access article distributed under the terms and conditions of the Creative Commons Attribution (CC BY) license.

for defining recovery but also for generating pectin fractions with deliberately different molecular states.

Citric acid was selected for its food compatibility and established use with passion-fruit peel [3]. Compared with nitric and sulfuric acids, it has yielded less pectin but higher esterification, molar mass, and gel strength [4]. Other organic acids offer different trade-offs: malic and tartaric acids produced high-methoxyl apple pectins, but citric acid pectin had greater molar mass and viscosity [8]; microwave extraction of passion-fruit peel with tartaric acid improved recovery relative to acetic acid but reduced purity and esterification [9]. These findings motivate the choice without establishing universal superiority.

Film formation provides one test of bulk-network assembly. During drying, pectin chains must form a continuous matrix around the plasticizer and remaining water. Mechanical strength and stiffness can decrease when extensive chain scission lowers intermolecular connectivity, but molar mass is not an isolated predictor: chain conformation, methyl esterification, branching, plasticizer distribution, and packing also influence cohesion and fracture [10]. A recent comparison of two lemon-peel pectins even showed that the lower-molar-mass fraction formed the stronger film, illustrating that an optimum cannot be defined from chain size alone [11]. Pectin source and molecular architecture must therefore be considered together with strength, flexibility, water-vapor transport, and water solubility [12,13].

Emulsion stabilization probes a different assembly pathway. Pectin-rich extracts may contribute through adsorption at the oil–water interface, electrostatic and steric repulsion, and increased viscosity of the aqueous phase [14]. These mechanisms are source- and structure-dependent, and ζ-potential alone does not quantify adsorbed mass, interfacial-layer thickness, or resistance to gravitational migration [15,16]. Studies of tailored citrus pectins have further shown that the influence of esterification depends on molar-mass range and that controlled depolymerization can sometimes improve adsorption, whereas excessive depolymerization can weaken steric and bulk-phase stabilization [17,18]. Particulate adsorption at the interface was not demonstrated; therefore, a Pickering stabilization mechanism is not assigned to these emulsions.

Most studies optimize an extraction response or evaluate a single downstream application. Fewer compare how fractions from the same feedstock and extraction series perform in two distinct assembly mechanisms under fixed formulations. Such a comparison can distinguish a genuine structure–function relationship from changes caused by botanical source or formulation composition. Films and emulsions were investigated separately: oil was included only in the emulsion system. The intended applications are pectin films for food packaging or produce coatings and emulsifiers for dispersed food systems; application performance on specific foods was not tested. These complementary tests of bulk cohesion and dispersion stability define the scope; gelation and other functional properties require separate evaluation.

The objective of this study was therefore to determine how extraction-induced differences among five representative yellow passion-fruit-peel pectins affected glycerol-plasticized films and sunflower-oil emulsions. It was hypothesized that mild extraction would retain sufficient chain continuity for strong, low-permeability films, whereas emulsion stability would be maximized by an intermediate balance of molecular size, charge, branching, and continuous-phase viscosity. Severe extraction was expected to increase negative charge while reducing both film-network formation and emulsion stability. The study was designed as application-level validation of selected fractions, not as a second optimization across the complete extraction series.

2. Materials and Methods

2.1. Raw Material, Extraction, and Experimental Unit

Fresh yellow passion fruits (*Passiflora edulis* Sims f. *flavicarpa*) were obtained from three independent commercial lots in Campina Grande, Paraíba, Brazil. Fruits were selected at commercial maturity based on a predominantly yellow peel and were excluded when presenting fungal decay, mechanical injury, insect damage, severe shriveling, or other visible defects. Harvest age in days after anthesis and individual fruit dimensions were unavailable because the fruits were commercially sourced. The fruits were washed under potable running water, immersed in a food-grade sodium hypochlorite solution containing 200 ppm free chlorine for 1 min, rinsed with potable water, and drained. The peels were manually separated from the pulp and seeds and dried in a convective drier at 50 °C for 24 h. Constant mass was defined as a relative mass change below 0.5% between two consecutive measurements performed 2 h apart after cooling the samples in a desiccator. The dried peels were milled, passed through a 60-mesh sieve, and stored at −20 °C.

Peel flour was extracted at a solid-to-liquid ratio of 1:20 (*w*/*v*) using 0, 0.086, 0.50, 2.0, or 10.0% (*w*/*v*) anhydrous citric acid at 75 °C and 200 rpm for 60 min. The hot suspension was filtered through 100 µm nylon fabric and centrifuged at 8000× *g* for 20 min at 20 °C. Pectin-rich material was precipitated by adding two volumes of absolute ethanol and holding the mixture at 4 °C for 24 h. The precipitate was recovered, washed three times with 70% ethanol and once with absolute ethanol, redissolved in water at 1% (*w*/*v*), dialyzed through a 3.5 kDa membrane until conductivity stabilized, frozen, and lyophilized. The water extraction was the process control. The five acid conditions were selected from an 11-level extraction study to span water-soluble, high-integrity, intermediate, low-methoxyl-transition, and severe-degradation regions. The fixed ratio corresponds to 1 g of flour per 20 mL of solution and permits comparison at a common solids loading; it was not optimized here. The 0.086% condition has literature precedent for retaining high esterification [3], while higher concentrations extend the severity range.

2.2. Molecular and Rheological Characterization of the Selected Fractions

The molecular and rheological descriptors were determined using the lyophilized fractions obtained independently from each of the three peel lots used for film and emulsion preparation. Samples were not pooled across lots. Technical measurements were averaged within each lot, providing three independent observations per extraction condition (n = 3). These descriptors were used for mechanistic interpretation and not as independent predictors in multivariable models.

2.2.1. Monosaccharide Composition and Structural Indices

Approximately 20 mg of dry, purified pectin-rich extract was mixed with 2 mL of 2 mol L^{-1} trifluoroacetic acid (TFA) in sealed glass tubes and hydrolyzed at 120 °C for 2 h. After cooling, the hydrolysate was neutralized with 2 mol L^{-1} NaOH, centrifuged at 5000× *g* for 10 min, and filtered through a 0.22 µm membrane. Galacturonic acid (GalA), rhamnose (Rha), arabinose (Ara), galactose (Gal), glucose, xylose, and mannose were determined using an Agilent 1260 Infinity HPLC system (Agilent Technologies, Santa Clara, CA, USA) equipped with a G1311C quaternary pump, G1329B autosampler, G1316A thermostated column compartment, and G1362A refractive-index detector. Separation was performed using a Hi-Plex H column (300 × 7.7 mm, 8 µm) protected by a PL Hi-Plex H guard column. The column was maintained at 70 °C, the detector at 40 °C, and 4 mmol L^{-1} sulfuric acid was used as the mobile phase at 0.6 mL min^{-1}. The injection volume was 10 µL. The monosaccharides were identified and quantified using individual external calibration curves. A reagent blank, a TFA-treated monosaccharide mixture, and commercial pectin subjected to the complete

hydrolysis procedure were included in every analytical batch. Results were corrected using experimentally determined hydrolysis recoveries. The recovery-corrected molar amount of monosaccharide was calculated using Equation (1).

$$n_{i,\mathrm{corr}} = \frac{\frac{m_i}{M_i}}{R_i} \quad (1)$$

where m_i is the HPLC-determined mass, M_i is the monosaccharide molar mass, and R_i is its fractional recovery. The structural indices were then calculated for each independent peel lot using Equations (2) and (3).

$$\mathrm{GalA/Rha} = \frac{n_{\mathrm{GalA,corr}}}{n_{\mathrm{Rha,corr}}} \quad (2)$$

and

$$(\mathrm{Ara} + \mathrm{Gal})/\mathrm{Rha} = \frac{n_{\mathrm{Ara,corr}} + n_{\mathrm{Gal,corr}}}{n_{\mathrm{Rha,corr}}} \quad (3)$$

GalA/Rha was interpreted as a comparative indicator of HG-rich relative to RG-I-rich backbone composition, whereas (Ara + Gal)/Rha represented the amount of RG-I-associated neutral side-chain sugars per rhamnose residue. Neither ratio was considered a direct measurement of domain length or branching architecture.

2.2.2. Apparent Titrimetric Degree of Esterification

Purified pectin-rich extract (0.200 g) was wetted with 2 mL of ethanol and dispersed in 20 mL of water at 40 °C for 2 h. Free carboxyl groups were titrated with standardized 0.100 mol L^{-1} NaOH to pH 8.30 using a 905 Titrando automatic titrator (Metrohm, Herisau, Switzerland), and the consumed volume was recorded as V_1. The titration–saponification principle is supported by established pectin analyses [19].

Esterified carboxyl groups were saponified by adding 10.00 mL of 0.100 mol L^{-1} NaOH and agitating the sample for 2 h. Subsequently, 10.00 mL of 0.100 mol L^{-1} HCl was added, and the excess acid was back-titrated with 0.100 mol L^{-1} NaOH. The NaOH-equivalent volume associated with saponified ester groups was recorded as V_2. The apparent degree of esterification was calculated using Equation (4).

$$\mathrm{DE_{app}}(\%) = 100\,\frac{V_2}{V_1 + V_2} \quad (4)$$

The simplified expression applies because all titrants had the same molar concentration. Because alkali-labile acetyl groups may also contribute to V_2, we described the result as apparent titrimetric DE rather than specifically as the degree of methyl esterification. Because citric acid was used during extraction, only the ethanol-washed, dialyzed, and lyophilized fractions were titrated. Before titration, residual citrate was extracted by dispersing 100 mg of purified sample in 10 mL of ultrapure water for 1 h at 25 °C. The suspension was centrifuged at 10,000× g for 15 min and filtered through a 0.22 µm membrane. Citrate was determined with the Agilent 1260 Infinity HPLC system and Hi-Plex H column described above, using a G1315D diode-array detector at 210 nm, 4 mmol L^{-1} sulfuric acid at 0.6 mL min^{-1}, and a column temperature of 70 °C. Recovery was verified using matrix spikes equivalent to 0.10, 0.50, and 2.00% (w/w) of dry extract, and residual citrate was confirmed to be below 2% of the total titratable acid equivalents.

2.2.3. Intrinsic Viscosity and Apparent Viscosity-Average Molar Mass

Five pectin concentrations ranging from 0.10 to 0.50 g dL^{-1} were prepared in 0.10 mol L^{-1} NaCl containing 0.05% (w/v) EDTA at pH 7.0. Solutions were hydrated

for 12 h, centrifuged at 10,000× g, and filtered through 0.45 µm membranes. Flow times were measured using a Cannon–Ubbelohde No. 1C capillary viscometer (Cannon Instrument Company, State College, PA, USA) maintained at 25.00 ± 0.05 °C in a TE-184 thermostatic bath (Tecnal, Piracicaba, Brazil) [20]. Solvent and sample flow times were measured in triplicate.

Relative viscosity and specific viscosity were calculated using Equations (5) and (6).

$$\eta_r = \frac{t}{t_0} \tag{5}$$

and

$$\eta_{sp} = \eta_r - 1 \tag{6}$$

where t and t_0 are the sample and solvent flow times, respectively. Intrinsic viscosity, $[\eta]$, was obtained from the common zero-concentration intercept of the Huggins and Kraemer relationships, as presented by Equations (7) and (8). Here, c is pectin concentration (g dL^{-1}), $[\eta]$ is expressed in dL g^{-1}, and k_H and k_K are the fitted dimensionless concentration coefficients.

$$\frac{\eta_{sp}}{c} = [\eta] + k_H[\eta]^2 c \tag{7}$$

$$\frac{ln\ \eta_r}{c} = [\eta] + k_K[\eta]^2 c \tag{8}$$

Apparent viscosity-average molar mass was calculated from the Mark–Houwink relationship using Equations (9) and (10):

$$[\eta] = K{M_v}^a \tag{9}$$

$$M_v = \left(\frac{[\eta]}{K}\right)^{1/a} \tag{10}$$

The available Mark–Houwink constants for pectin in water do not reproduce the tabulated $[\eta]$–M_v pairs obtained in the NaCl–EDTA solvent. Therefore, $[\eta]$ is the directly supported hydrodynamic descriptor, and M_v should not be interpreted as absolute M_w. K and a are the solvent- and temperature-dependent Mark–Houwink coefficient and exponent, respectively.

2.2.4. Steady-Shear Rheology and Cross-Model Fitting

Standardized dispersions containing 2.0% (w/v) pectin-rich fraction were prepared in 0.10 mol L^{-1} NaCl containing 0.05% (w/v) EDTA at pH 7.00 ± 0.05. The dispersions were heated at 80 °C for 15 min, cooled to room temperature, and hydrated for 12 h before measurement. Flow curves were obtained at 25 °C using a HAAKE MARS 60 rheometer (Thermo Fisher Scientific, Karlsruhe, Germany) equipped with 35 mm serrated parallel plates, a 1.0 mm gap, and a solvent trap. After 5 min of equilibration, apparent viscosity was recorded over a shear-rate range of 0.1–1000 s^{-1}. The flow curve from each independent peel lot was fitted separately by nonlinear regression in GraphPad Prism 10 (GraphPad Software, Boston, MA, USA) using the Cross model (Equation (11)) described by Cross (1965) [21,22].

$$\eta(\dot{\gamma}) = \eta_\infty + \frac{\eta_0 - \eta_\infty}{1 + (\lambda\dot{\gamma})^m} \tag{11}$$

where $\eta(\dot{\gamma})$ is apparent viscosity at shear rate $\dot{\gamma}$, η_0 and η_∞ are the limiting zero- and infinite-shear viscosities, respectively, λ is the characteristic time constant, and m is the dimensionless Cross exponent. The lot-specific fitted values of η_0 were retained for sta-

tistical analysis. Because η_0 was model-derived, it was described as 'Cross-estimated zero-shear viscosity'.

The selected fractions were qualified using descriptors generated in the same experimental campaign. GalA/Rha and (Ara + Gal)/Rha were calculated on a molar basis from recovery-corrected monosaccharide profiles obtained by TFA hydrolysis and HPLC. Potentiometric degree of esterification (DE) was obtained by neutralization of free carboxyl groups followed by saponification and back-titration. Intrinsic viscosity was determined in 0.10 mol L^{-1} NaCl containing 0.05% EDTA at pH 7.0 and 25 °C; apparent viscosity-average molar mass (M_v) was calculated using the Mark–Houwink relationship and is interpreted comparatively rather than as absolute M_w [20]. Zero-shear viscosity (η_0) was obtained by fitting the Cross model to 2.0% (w/v) standardized dispersions [22].

2.3. Film Preparation

Film-forming dispersions contained 2.0% (w/v) pectin-rich fraction and glycerol equivalent to 30% of polymer dry mass. Dispersions were heated at 80 °C for 15 min, degassed, and cast at a constant dry-solid loading of 0.010 g cm^{-2}. Films were dried at 40 °C for 24 h and conditioned at 25 ± 2 °C and 50 ± 5% relative humidity for 48 h before analysis [23].

2.4. Film Characterization

Film thickness was measured at ten positions using a digital micrometer. Tensile strength, elongation at break, and Young's modulus were determined according to ASTM D882 [24] using a TA.XTplusC texture analyzer (Stable Micro Systems, Godalming, UK) equipped with tensile grips, a 50 mm initial grip separation, and a crosshead speed of 1 mm s^{-1}. Puncture resistance was measured using the same instrument. Water-vapor permeability (WVP) was determined gravimetrically according to ASTM E96/E96M [25]. Film moisture, water solubility, and opacity were also determined. Technical readings were averaged within each independently extracted peel lot before statistical analysis [26]. Related pectin-film characterization procedures are described by Jiang et al. [27].

2.5. Emulsion Preparation

The aqueous phase contained 1.0% (w/w) pectin-rich fraction and 10 mmol L^{-1} NaCl and was adjusted to pH 7.0. Refined sunflower oil constituted 10% (w/w) of the emulsion. A coarse emulsion was prepared using an Ultra-Turrax T25 homogenizer (IKA, Staufen, Germany) at 12,000 rpm for 2 min, followed by two passes at 50 MPa through an LM-200 high-pressure homogenizer (Microfluidics, Westwood, MA, USA). Each independent extract generated one independent emulsion batch. Related pectin-emulsion preparation and droplet-characterization methods are reported by Shuai et al. [28]; the formulation and processing settings used here are specified above.

2.6. Emulsion Characterization and Storage

Emulsions were stored at 25 °C for 21 days. Droplet-size distributions were measured on days 0, 1, 7, 14, and 21 using a Mastersizer 3000 laser-diffraction analyzer (Malvern Instruments, Malvern, UK), and D[3,2], D[4,3], and span were recorded. ζ-potential was measured using a Zetasizer Nano ZS (Malvern Instruments, Malvern, UK) after dilution in the corresponding continuous phase. We also assessed creaming index, optical microscopy, apparent viscosity, and storage-dependent changes in droplet diameter. The available planning summaries used for statistical comparisons contain D[4,3] at days 0 and 21; D[3,2] and span are not reported here. Optical micrographs were acquired on days 0 and 21 to qualitatively assess droplet morphology and clustering.

2.7. Statistical Analysis

Exploratory one-way ANOVA and Tukey's honestly significant difference (HSD) tests were calculated directly from the reported means, sample SDs, and $n = 3$ per extraction condition using SciPy 1.18.1. Under an independent-groups model with normal errors and equal variances, the pooled error mean square was $\Sigma(n_i - 1)s_i^2/\Sigma(n_i - 1)$, with ANOVA degrees of freedom 4 and 10. Each response was a separate family of ten pairwise comparisons; Tukey-adjusted $p < 0.05$ indicated a detected difference, without further adjustment across responses. For equal group sizes, $q = |\text{mean}_i - \text{mean}_j| / \sqrt{(\text{MSE}/3)}$, with critical $q = 4.6543$. Day 0 and day 21 endpoints were analyzed separately, and the reported growth-ratio means and SDs were analyzed as a separate response. These exploratory calculations do not account for matching of extraction conditions within peel lots or repeated observations during storage; normality and equal variances were assumed rather than verified from individual observations.

3. Results

3.1. Selected Fractions Represented Distinct Molecular States

The five fractions covered a broad structural range while keeping botanical source, extraction temperature, residence time, solid-to-liquid ratio, purification, and drying history constant (Table 1). The water, 0.086%, and 0.50% fractions remained high methoxyl and presented apparent M_v values of approximately 210–255 kDa. The 2.0% fraction crossed into low-methoxyl behavior while retaining an intermediate apparent M_v of approximately 140 kDa. The 10.0% fraction combined the lowest DE and apparent M_v with the greatest GalA/Rha ratio and least retained RG-I-associated side-chain contribution. The increase in GalA/Rha at severe extraction must not be interpreted as improved molecular quality because it coincided with absolute sugar losses and extensive chain shortening in the companion mass-balance study. The selected fractions differed markedly in esterification, chain size, branching, and zero-shear viscosity (Table 1).

Table 1. Molecular and rheological descriptors of the selected pectin-rich fractions.

Citric Acid (% *w*/*v*)	GalA/Rha (Molar)	(Ara + Gal)/Rha (Molar)	DE (%)	Apparent M_v (kDa)	η_0 at 2% (Pa·s)
0	4.39 ± 0.37^{c}	2.40 ± 0.21^{a}	72 ± 2^{ab}	220 ± 15^{ab}	6.3 ± 0.8^{b}
0.086	5.90 ± 0.44^{bc}	2.28 ± 0.19^{a}	79 ± 2^{a}	255 ± 18^{a}	11.8 ± 1.4^{a}
0.50	7.87 ± 0.60^{b}	2.02 ± 0.17^{ab}	68 ± 3^{b}	210 ± 18^{b}	12.4 ± 1.5^{a}
2.0	10.08 ± 0.86^{a}	1.69 ± 0.15^{b}	47 ± 4^{c}	140 ± 18^{c}	7.4 ± 1.0^{b}
10.0	11.48 ± 1.23^{a}	0.83 ± 0.09^{c}	20 ± 5^{d}	55 ± 12^{d}	1.4 ± 0.2^{c}

Values are planning means ± SD ($n = 3$ independent peel lots). Apparent M_v is a comparative Mark–Houwink estimate; η_0 is the Cross-model zero-shear viscosity. Within each column, means without a shared superscript letter differ by Tukey HSD (adjusted $p < 0.05$); shared letters indicate no detected difference, not equivalence. Letters are based on the exploratory independent-groups summary analysis described in Section 2.7.

This design separates two related effects of acid severity. Mild acidification selected a more highly esterified, hydrodynamically large pectin population, whereas increasingly severe extraction progressively exposed free carboxyl groups and reduced chain size and branching [29]. Across multiple sources, less acidic extraction conditions yield pectin with higher degrees of methylation or esterification and larger molecular weights. In citrus pectin, as pH rose from 1.0 toward 7.0, molecular weight increased, and the degree of esterification rose, with the HG region expanding from ~75% to ~85% [30]. The resulting fractions provide a controlled within-source test of whether application performance tracks charge, molecular integrity, or a combination of both.

The non-monotonic transition from water extraction to 0.086% acid suggests that the early part of the series was governed by selective solubilization before molecular degradation became dominant. Water likely recovered pectin already accessible to the solvent, whereas mild acidification and citrate-mediated disruption of ionic associations may have released a larger, more highly esterified population, accounting for the higher apparent M_v and DE at 0.086% [31]. With further acidification, proton-catalyzed glycosidic cleavage and preferential erosion of neutral-sugar-rich RG-I regions likely outweighed this release effect. The simultaneous increase in GalA/Rha and decrease in both (Ara + Gal)/Rha and apparent M_v therefore indicate relative HG enrichment through side-chain and chain loss, rather than formation of a more intact or intrinsically higher-quality pectin. Each recovered fraction should consequently be considered the combined outcome of selective solubilization and modification within the hot acidic medium [30].

3.2. Mild Extraction Preserved Load-Bearing Film Networks

All eight film responses differed among extraction conditions in the exploratory independent-groups ANOVA ($p < 0.05$). The largest contrasts occurred in tensile strength and Young's modulus. Because polymer concentration, glycerol-to-polymer ratio, dry-solid loading, drying, and conditioning were held constant, the pattern is consistent with extraction-induced differences among the pectin-rich fractions. Mechanical resistance declined under severe extraction, whereas elongation, solubility, and WVP increased (Table 2, Figure 1).

Table 2. Mechanical, barrier, and water-response properties of films prepared from representative passion-fruit-peel pectins.

Property	0%	0.086%	0.50%	2.0%	10.0%
Tensile strength (MPa)	27.92 ± 2.73 ^{ab}	31.26 ± 3.00 ^{a}	24.68 ± 2.47 ^{b}	14.80 ± 1.68 ^{c}	3.34 ± 0.77 ^{d}
Elongation at break (%)	14.44 ± 2.44 ^{c}	12.71 ± 2.27 ^{c}	17.56 ± 2.76 ^{bc}	25.41 ± 3.54 ^{b}	34.66 ± 4.47 ^{a}
Young's modulus (MPa)	418.8 ± 41.9 ^{ab}	468.9 ± 46.9 ^{a}	370.2 ± 37.0 ^{b}	222.0 ± 22.2 ^{c}	50.1 ± 5.0 ^{d}
Puncture resistance (N)	7.30 ± 0.68 ^{a}	7.89 ± 0.73 ^{a}	6.83 ± 0.65 ^{ab}	5.29 ± 0.52 ^{b}	3.51 ± 0.38 ^{c}
WVP ($\times 10^{-10}$ g m m^{-2} s^{-1} Pa^{-1})	2.70 ± 0.27 ^{b}	1.70 ± 0.17 ^{c}	1.82 ± 0.18 ^{c}	2.90 ± 0.29 ^{b}	4.70 ± 0.47 ^{a}
Water solubility (%)	34.0 ± 2.7 ^{d}	38.5 ± 3.1 ^{cd}	46.0 ± 3.7 ^{bc}	53.5 ± 4.3 ^{ab}	58.5 ± 4.7 ^{a}
Opacity	3.90 ± 0.31 ^{bc}	3.15 ± 0.25 ^{c}	3.24 ± 0.26 ^{bc}	4.05 ± 0.32 ^{b}	5.40 ± 0.43 ^{a}
Moisture (%)	10.08 ± 0.50 ^{a}	9.72 ± 0.49 ^{ab}	9.12 ± 0.46 ^{abc}	8.52 ± 0.43 ^{bc}	8.12 ± 0.41 ^{c}

Values are mean ± SD ($n = 3$ independent peel lots). WVP is expressed as $\times 10^{-10}$ g m m^{-2} s^{-1} Pa^{-1}. Within each row, means without a shared superscript letter differ by Tukey HSD (adjusted $p < 0.05$); shared letters indicate no detected difference, not equivalence. Letters are based on the exploratory independent-groups summary analysis described in Section 2.7.

Extraction condition affected tensile strength ($F_{4,10} = 74.40$, $p < 0.001$), elongation at break ($F_{4,10} = 24.13$, $p < 0.001$), Young's modulus ($F_{4,10} = 74.41$, $p < 0.001$), and puncture resistance ($F_{4,10} = 25.62$, $p < 0.001$). Tukey-adjusted comparisons placed the water, 0.086%, and 0.50% films in an overlapping high-strength region, although the 0.086% film had greater tensile strength and modulus than the 0.50% film ($p_{adj} = 0.034$ for both responses). Mechanical resistance subsequently decreased at 2.0% and reached its lowest level at 10.0% acid. WVP was also affected by extraction condition ($F_{4,10} = 49.47$, $p < 0.001$); the 0.086% and 0.50% films formed the lowest-WVP statistical group and did not differ from one another ($p_{adj} = 0.986$).

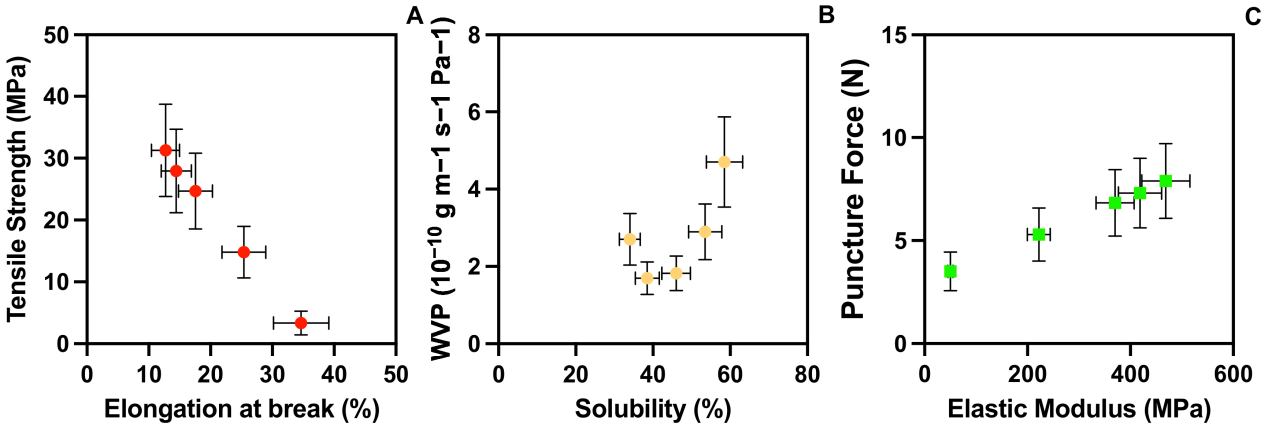

Figure 1. Film-property relationships: (**A**) tensile strength versus elongation at break; (**B**) WVP versus water solubility; and (**C**) puncture resistance versus Young's modulus. Points show mean ± SD (n = 3).

The water, 0.086%, and 0.50% fractions formed a high-strength region. Tensile strength was 27.92 ± 2.73 MPa for the water-extracted fraction, 31.26 ± 3.00 MPa at 0.086% acid, and 24.68 ± 2.47 MPa at 0.50%, with the 0.086% film stronger than the 0.50% film (Tukey-adjusted p = 0.034), while the water control did not differ from either. Strength decreased to 14.80 ± 1.68 MPa at 2.0% and 3.34 ± 0.77 MPa at 10.0% acid. Young's modulus followed the same trend, decreasing from 370.2–468.9 MPa for the water and mild-acid films to 222.0 MPa at 2.0% and 50.1 MPa at 10.0%. Puncture resistance similarly decreased from approximately 7–8 N to 3.51 N across the extraction series.

The severe-acid loss of strength, stiffness, and puncture resistance is consistent with insufficient chain continuity for a cohesive load-bearing network. Longer chains can provide more potential contact and entanglement sites during solvent evaporation, while retained side chains and ester groups can change conformation, hydrophobic association, hydrogen bonding, and plasticizer distribution. The present fractions changed in all of these attributes simultaneously, so apparent M_v should be treated as an integrated marker of extraction damage rather than the only causal variable. This caution is supported by the contrasting lemon-pectin study of Chandrasekar et al. (2026), in which a lower-M_v fraction formed a stronger film because packing and conformation outweighed chain length [11].

The coordinated loss of tensile strength, Young's modulus, and puncture resistance, accompanied by increasing elongation at break, is consistent with a decline in effective load-bearing junction density [23,32]. High-integrity chains can bridge multiple intermolecular contact zones and redistribute stress through topological overlap, hydrogen bonding, and methyl-ester-associated interactions [33]. Once scission shortens the chains, the same glycerol-to-polymer ratio acts on a network containing fewer spanning connections and more mobile chain ends. Segmental mobility can therefore increase while resistance to crack initiation and propagation decreases. This provides a mechanistic distinction between flexibility and toughness: the 10.0% film deformed further because its network was weak, not necessarily because it dissipated more energy before fracture [34]. Nevertheless, chain size should not be treated as sufficient on its own because differences in conformation and packing can allow a lower-molar-mass pectin to form a stronger film, as recently demonstrated for differently extracted lemon pectins [11].

Elongation at break changed in the opposite direction, increasing from 12.71–17.56% in the 0.086–0.50% films to 25.41% at 2.0% and 34.66% at 10.0% acid. Greater elongation did not indicate improved toughness: the 10.0% film combined high extensibility with the lowest strength, modulus, and puncture resistance. It was therefore weak and readily deformable, not a robust flexible material. Among the tested fractions, 0.50% provided the

most balanced strength–flexibility combination, while 0.086% gave the largest strength and modulus means.

3.3. Film Barrier and Water Response Showed an Intermediate Optimum

WVP exhibited a U-shaped response (Figure 1B). The mean decreased from 2.70 ± 0.27 × 10^{-10} g m m^{-2} s^{-1} Pa^{-1} in the water-control film to 1.70 ± 0.17 and 1.82 ± 0.18 × 10^{-10} at 0.086 and 0.50% acid, respectively. It then increased to 2.90 ± 0.29 × 10^{-10} at 2.0% and 4.70 ± 0.47 × 10^{-10} at 10.0%. The summary-statistic analysis did not statistically separate the two mild-acid films. Extraction condition affected WVP ($F_{4,10}$ = 49.47, p = 1.48 × 10^{-6}), water solubility ($F_{4,10}$ = 21.75, p = 6.39 × 10^{-5}), and opacity ($F_{4,10}$ = 23.80, p = 4.29 × 10^{-5}). Tukey-adjusted comparisons showed that the 0.086% and 0.50% films formed the lowest-WVP statistical group and did not differ from one another (adjusted p = 0.986). WVP subsequently increased at 2.0% and 10.0% acid, while solubility generally increased across the extraction series.

The U-shaped WVP response can be interpreted as a sorption–diffusion trade-off. Water-vapor permeability depends on both the amount of water sorbed by the matrix and that water's mobility through the film. Mild extraction may have favored packing and reduced the effective diffusion coefficient by producing a continuous, low-defect matrix. In lemon-peel pectin, microwave-assisted extraction produced flexible small random coils that packed efficiently, creating a cohesive network with better water contact angles than the higher-molecular-weight ultrasonic counterpart [11]. In contrast, severe de-esterification increased the availability of polar carboxyl groups, while chain scission increased chain ends, free volume, and local discontinuities [35]. This combination could increase water affinity and diffusional mobility even though the equilibrium moisture content decreased slightly. Moisture content and WVP therefore need not vary in parallel: the former represents one conditioned equilibrium state, whereas WVP describes transport across a chemical-potential gradient. Pectin films with phenolic acids showed reduced water content but increased diffusion coefficients and WVP, confirming that equilibrium moisture and transport rate are decoupled [36]. The concurrent increases in solubility, opacity, and WVP at 10.0% acid are consistent with a more heterogeneous and readily hydrated matrix, although sorption isotherms, cross-sectional microscopy, contact-angle measurements, and thermal analysis are required to test this mechanism [27,37]. The lower WVP of the 0.086–0.50% films is consistent with a more continuous matrix and a longer diffusion path, whereas the rise after severe extraction suggests discontinuities, greater free volume, or altered plasticizer–polymer organization. These explanations remain hypotheses until film cross-sections, surface morphology, contact angle, and thermal transitions are measured. Because water-vapor transport also depends strongly on thickness and water activity, direct comparison should be restricted to films tested under the same verified ASTM conditions.

Water solubility increased from 34.0 ± 2.7% for the water-extracted film to 58.5 ± 4.7% at 10.0% acid. The 2.0 and 10.0% films were more soluble than the water and 0.086% films in the summary-statistic Tukey comparisons. The response is consistent with shorter chains, greater carboxyl availability, and weaker network connectivity, but residual low-molar-mass material and glycerol distribution should also be considered. Opacity was lowest for the 0.086 and 0.50% films and increased to 5.40 ± 0.43 at 10.0%, while film moisture declined only modestly.

3.4. Emulsion Formation Was Best at Intermediate Extraction Severity

Initial D[4,3] decreased from 2.41 ± 0.14 μm in the water-control emulsion to 1.95 ± 0.12 μm at 0.086% and reached the smallest mean, 1.72 ± 0.10 μm, at 0.50% acid.

D[4,3] then increased to 2.08 ± 0.12 µm at 2.0% and 3.50 ± 0.21 µm at 10.0%. The 0.50% emulsion had smaller initial droplets than the water and 10.0% systems, whereas 10.0% produced larger droplets than all other treatments in the summary-statistic Tukey comparisons. Extraction condition affected initial D[4,3] ($F_{4,10}$ = 71.50, p < 0.001), day 21 D[4,3] ($F_{4,10}$ = 158.89, p < 0.001), ζ-potential ($F_{4,10}$ = 34.20, p < 0.001), η_{50} ($F_{4,10}$ = 18.15, p < 0.001), and day 21 creaming ($F_{4,10}$ = 86.73, p < 0.001). At day 0, the 0.50% emulsion had smaller droplets than the water and 10.0% systems but did not differ from the 0.086% or 2.0% treatments. At day 21, the 0.50% and 0.086% emulsions did not differ significantly in day 21 droplet size (Tukey-adjusted p = 0.168), whereas the 10.0% fraction produced the largest droplets and greatest creaming. The 0.086% and 0.50% emulsions also formed the highest-viscosity region. Figure 2 presents the emulsion droplet changes.

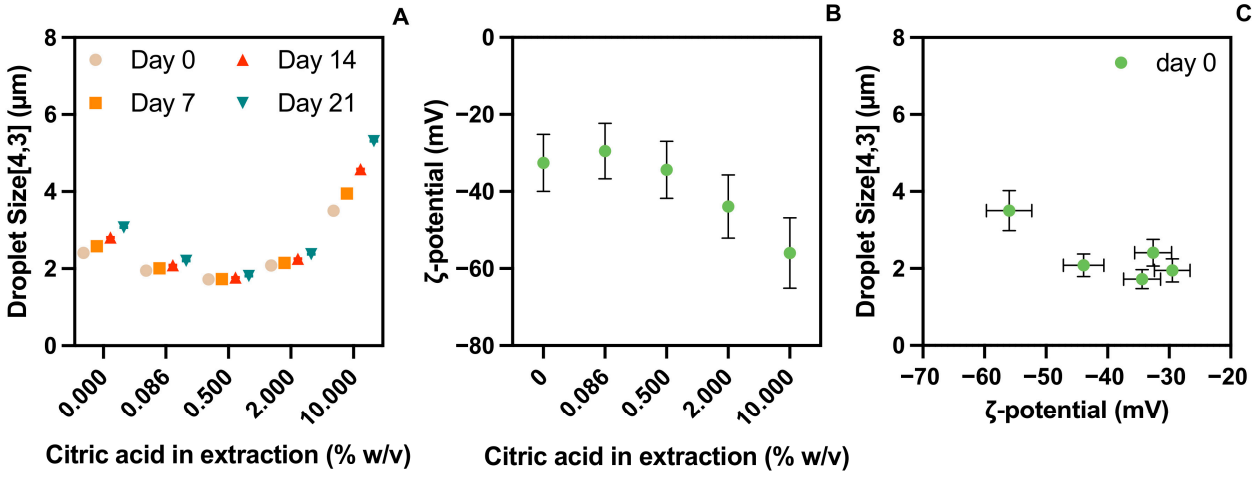

Figure 2. Emulsion droplet size and charge: (**A**) D[4,3] during storage; (**B**) ζ-potential; and (**C**) day 0 D[4,3] versus ζ-potential. Values are mean ± SD (n = 3).

The 0.50% emulsion produced the smallest droplets and lowest creaming, whereas 10.0% showed the greatest destabilization (Table 3). The minimum initial droplet size at 0.50% acid suggests a kinetic optimum during homogenization rather than a simple maximum in electrostatic stabilization. Droplet formation is governed by competition between disruptive stresses and recoalescence before the newly generated interface is fully covered [38]. A very large pectin molecule may provide strong steric and bulk-phase stabilization after adsorption but diffuse and rearrange comparatively slowly at a rapidly expanding interface. Conversely, severely depolymerized chains may reach the interface rapidly but form a thin and weakly viscoelastic layer [39]. The 0.50% fraction may therefore occupy an intermediate regime in which molecular mobility permits sufficiently rapid coverage while chain dimension, RG-I-associated side chains, and solution viscosity remain adequate to suppress recoalescence [40]. This interpretation agrees with citrus-pectin studies showing that controlled depolymerization can improve surface activity, whereas very-low-molar-mass products lose viscosity-building capacity and become susceptible to flocculation and coalescence [41].

The droplet-size result cannot be explained by ζ-potential alone. The 10.0% fraction had the greatest magnitude of negative charge (−56.0 ± 3.7 mV) but produced the largest droplets. Conversely, the 0.086% fraction had the least negative ζ-potential (−29.5 ± 2.9 mV) and still formed comparatively small droplets. Pectin emulsification depends on adsorption kinetics, conformation, hydrophobic or proteinaceous moieties, steric-layer dimensions, and bulk rheology, not simply diffuse-layer potential [17,28]. The current experiment did not measure dynamic interfacial tension or adsorbed mass, so interfacial mechanisms must remain interpretive. The 10.0% fraction combined the most

negative ζ-potential with the largest droplets, showing that charge alone did not determine emulsion formation (Figure 2A–C).

Table 3. Formation and 21-day stability of oil-in-water emulsions stabilized by representative passion-fruit-peel pectins.

Property	0%	0.086%	0.50%	2.0%	10.0%
D[4,3], day 0 (μm)	2.41 ± 0.14 ^{b}	1.95 ± 0.12 ^{c}	1.72 ± 0.10 ^{c}	2.08 ± 0.12 ^{bc}	3.50 ± 0.21 ^{a}
D[4,3], day 21 (μm)	3.07 ± 0.18 ^{b}	2.20 ± 0.13 ^{cd}	1.81 ± 0.11 ^{d}	2.38 ± 0.14 ^{c}	5.31 ± 0.32 ^{a}
D[4,3] growth ratio	1.274 ± 0.102 ^{ab}	1.130 ± 0.090 ^{b}	1.050 ± 0.084 ^{b}	1.146 ± 0.092 ^{b}	1.514 ± 0.121 ^{a}
ζ-potential (mV)	−32.6 ± 3.0 ^{a}	−29.5 ± 2.9 ^{a}	−34.4 ± 3.0 ^{a}	−43.9 ± 3.3 ^{b}	−56.0 ± 3.7 ^{c}
η_{50} (Pa·s)	0.0489 ± 0.0049 ^{cd}	0.0654 ± 0.0065 ^{ab}	0.0672 ± 0.0067 ^{a}	0.0522 ± 0.0052 ^{bc}	0.0342 ± 0.0034 ^{d}
Creaming at day 21 (%)	14.6 ± 2.0 ^{b}	6.5 ± 1.1 ^{cd}	2.0 ± 0.7 ^{d}	7.4 ± 1.2 ^{c}	28.1 ± 3.3 ^{a}

Values are planning means ± SD (n = 3 independent peel lots). The growth ratio is D[4,3] at day 21 divided by D[4,3] at day 0. Statistical comparisons use the day-0 and day-21 D[4,3] summaries; D[3,2], span, and mixed-model contrasts are not reported. Within each row, means without a shared superscript letter differ by Tukey HSD (adjusted $p < 0.05$); shared letters indicate no detected difference, not equivalence. Letters are based on the exploratory independent-groups summary analysis described in Section 2.7.

The apparently paradoxical behavior of the 10.0% fraction can be resolved by separating electrostatic potential from interfacial-layer architecture. At pH 7, its low DE provides numerous ionized carboxyl groups and, consequently, a strongly negative ζ-potential, but ζ-potential does not measure adsorbed mass, interfacial-layer thickness, interfacial elasticity, or anchoring strength [42]. Moreover, 10 mmol L^{-1} NaCl partially screens long-range electrostatic interactions, increasing the relative importance of steric protection and continuous-phase viscosity. Loss of RG-I-associated side chains may have reduced the thickness of the hydrated steric corona, while the low apparent M_v and η_{50} decreased resistance to droplet collisions and gravitational migration. Studies of pectin at oil–water interfaces show that HG and RG domains adopt different interfacial configurations and that hydrophobic, acetylated, or proteinaceous moieties can contribute to anchoring. A highly charged but short and weakly anchored layer may consequently be less protective than a moderately charged, thicker, and more viscoelastic layer [28,43]. In purple passion-fruit pectin, steam-explosion-assisted extraction, with or without ultrasound, improved storage stability relative to ultrasound-assisted extraction alone [5]. Together with the film comparison [11], this illustrates application-dependent benefits rather than a universally superior extraction route.

Apparent viscosity at 50 s^{-1} was largest for the 0.086 and 0.50% emulsions, approximately 0.065–0.067 Pa·s, and smallest for the 10.0% emulsion, 0.0342 Pa·s. A more viscous continuous phase can reduce gravitational migration and collision frequency and may partly explain why the 0.50% emulsion combined small droplets with low creaming [44]. Bulk viscosity can also alter energy dissipation during homogenization; consequently, the smaller initial droplets cannot be assigned uniquely to faster interfacial adsorption. Measuring interfacial tension alongside matched-viscosity controls would separate these contributions [45].

3.5. Storage Stability Depended on the Balance Between Molecular Integrity, Charge, and Viscosity

After 21 days, D[4,3] was 3.07 ± 0.18 μm for the water-control emulsion, 2.20 ± 0.13 μm at 0.086%, 1.81 ± 0.11 μm at 0.50%, 2.38 ± 0.14 μm at 2.0%, and 5.31 ± 0.32 μm at 10.0%. In the exploratory Tukey analysis, the 10.0% fraction had larger day 21 droplets than all other fractions. The 0.50% fraction had smaller droplets than the water and 2.0% fractions but did not differ from 0.086% (adjusted p = 0.168). The supplied growth-ratio summaries also differed among extraction conditions ($F_{4,10}$ = 10.16, p = 0.00151); the 10.0% ratio ex-

ceeded those at 0.086%, 0.50%, and 2.0% but did not differ from the water control. These relationships are illustrated in Figure 3A–C.

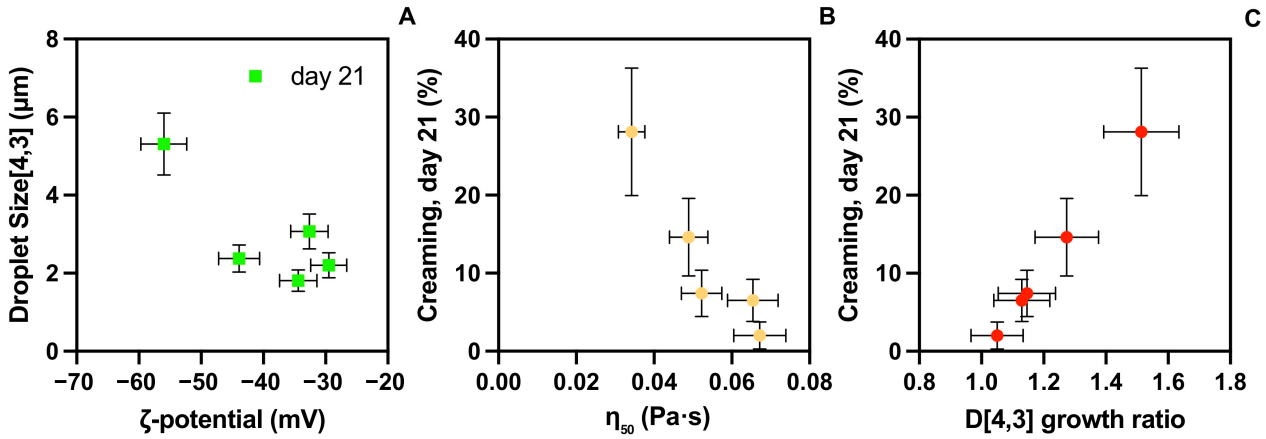

Figure 3. Day 21 emulsion stability: (**A**) D[4,3] versus ζ-potential; (**B**) creaming versus η_{50}; and (**C**) creaming versus D[4,3] growth ratio. Points show mean ± SD (n = 3).

The increase in D[4,3] should be described as apparent droplet growth rather than assigned directly to coalescence. Laser diffraction can report reversible flocs as larger objects unless the dilution and dispersion protocol disrupts them, whereas true coalescence irreversibly changes the primary droplet population. The 10.0% system is mechanistically compatible with both processes: its lower emulsion apparent viscosity may be associated with increased droplet mobility, while a thinner or less cohesive interfacial layer would reduce resistance to close approach and interfacial-film rupture. The available D[4,3] and creaming results therefore demonstrate destabilization but do not identify its microscopic pathway. Additional assessment of D[3,2], span, and particle size before and after controlled deflocculation would help distinguish aggregation from coalescence. Optical micrographs illustrate the droplet morphology of the emulsions at preparation and after 21 days of storage (Figure 4). In the displayed fields, the 0.50% fraction produced emulsions containing predominantly small droplets at both observation times. In contrast, the 10.0% fraction showed conspicuously large droplets and clusters, particularly on day 21. Clustering was also evident in the water-control and 2.0% emulsions after storage. These qualitative observations are consistent with the reported droplet-size results but do not establish statistical differences between treatments.

Creaming produced an even larger treatment contrast in the planning dataset. At day 21, creaming was 14.6 ± 2.0% for the water control, 6.5 ± 1.1% at 0.086%, 2.0 ± 0.7% at 0.50%, 7.4 ± 1.2% at 2.0%, and 28.1 ± 3.3% at 10.0% acid. Thus, the 0.50% fraction provided the most favorable provisional combination of droplet-size retention and resistance to macroscopic phase separation among the five selected fractions. However, the lower creaming mean at 0.50% was not significantly different from 0.086% in the exploratory Tukey comparison (adjusted p = 0.091).

The macroscopic creaming trend is directionally consistent with gravitational-separation theory, which predicts that migration velocity scales approximately with d^2/η. Using day 0 D[4,3] and η_{50} only as rough proxies, the expected velocity ratio between the 10.0% and 0.50% emulsions is $(3.50/1.72)^2 \times (0.0672/0.0342) \approx 8.1$. Thus, the larger droplets and lower viscosity of the 10.0% system act in the same direction and plausibly account for much of its greater day 21 creaming. This illustrative calculation is not a fitted prediction because D[4,3] is not a single-particle diameter, η_{50} is not the near-zero-shear viscosity governing gravitational motion, and interacting emulsions deviate from the ideal Stokes regime since ideal Stokes behavior applies to isolated spherical droplets in a stagnant

infinite fluid [46]. Mechanistically, it shows that electrostatic charge alone cannot compensate for the combined effects of large droplet size and low continuous-phase resistance. The most stable emulsions usually combine electrostatic repulsion with an elastic interfacial film, steric protection, or a thickened network that restricts droplet motion [47].

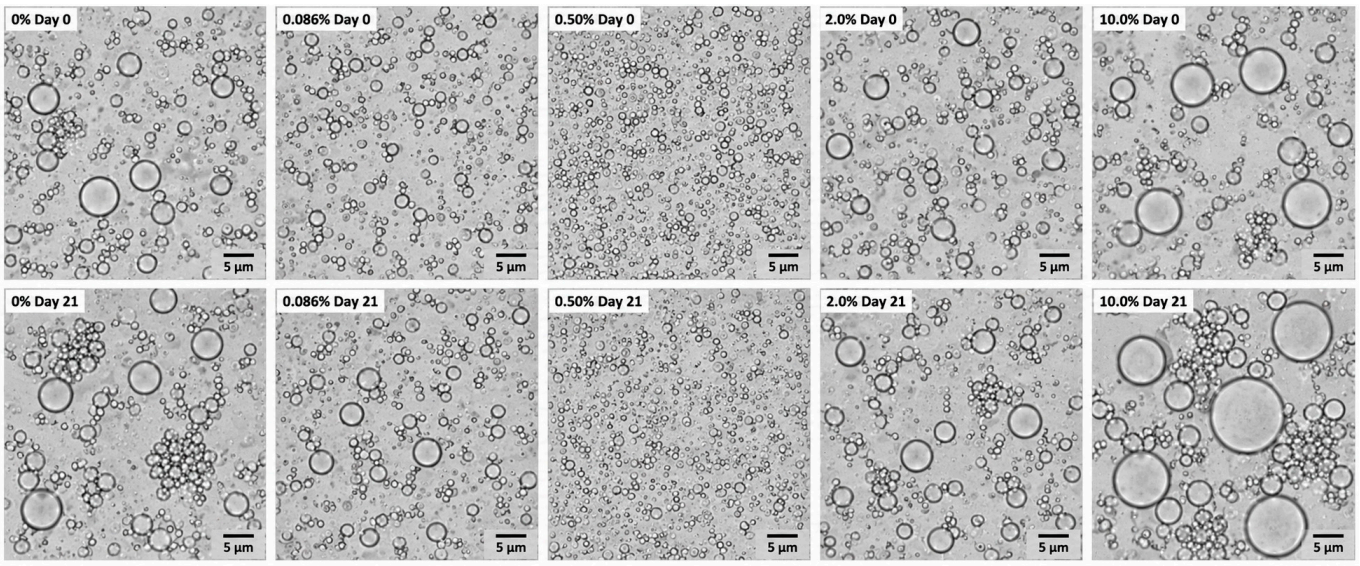

Figure 4. Optical micrographs of sunflower oil-in-water emulsions stabilized with yellow passion-fruit-peel pectin fractions extracted using different citric acid concentrations. Columns, from left to right, correspond to 0% (water extraction), 0.086%, 0.50%, 2.0%, and 10.0% (*w*/*v*) citric acid. The upper and lower rows show day 0 and day 21 of storage at 25 °C, respectively. Concentrations refer to the extraction solution, not the emulsion formulation. Scale bars: 5 µm.

The 0.50% fraction occupied an intermediate molecular state: high DE, apparent M_v near 210 kDa, retained RG-I-associated side chains, high solution and emulsion viscosity, and moderate negative charge. The 0.086% fraction retained greater apparent M_v but had a less negative ζ-potential; the 2.0% fraction had more free carboxyl groups but lower apparent M_v and viscosity. These comparisons support a balance model rather than a single-variable explanation. They do not establish a universal optimum molar mass. Tailored citrus-pectin systems have shown good emulsification at substantially lower molar masses, demonstrating that source, conformation, branching, protein, acetylation, formulation pH, ionic strength, and oil phase can shift the optimum [17]. These comparisons concern acid concentration; effects of lower or higher solid-to-liquid ratios cannot be inferred because that ratio was fixed.

4. Conclusions

Citric acid extraction generated yellow passion-fruit-peel pectins with markedly different application performance. Among the five selected fractions, 0.086% acid produced the largest film-strength and stiffness means, while 0.086–0.50% produced the lowest WVP. The 0.50% fraction provided the best overall emulsion response, combining small initial and day 21 droplets, high emulsion apparent viscosity, and minimal creaming. The 10.0% fraction performed poorly in both applications despite its strongly negative ζ-potential and high solubility, demonstrating that charge density could not compensate for severe loss of chain length and network-forming capacity. The results support an application-specific molecular-balance model. Film formation favored preserved chain continuity and cohesive dry-network assembly, whereas emulsion stabilization required a balance among molecular size, charge, conformation, and bulk-phase viscosity. No single extraction condition is

therefore universally optimal. Under the tested formulations, mild extraction at 0.086–0.50% citric acid was the most promising region for films and emulsions, while calcium-gel and recovery objectives belong to different extraction windows.

Author Contributions: Conceptualization, N.M., H.M.L. and M.A.B.P.; methodology, N.M., M.M.d.S., S.S.M., T.A.S.G., H.M.L. and M.A.B.P.; validation, N.M., M.M.d.S., S.B., S.S.M. and T.A.S.G.; formal analysis, N.M., H.M.L. and M.A.B.P.; investigation, N.M., M.M.d.S., S.B., S.S.M. and T.A.S.G.; resources, H.M.L. and M.A.B.P.; data curation, N.M., M.M.d.S., S.B. and H.M.L.; writing—original draft preparation, N.M. and H.M.L.; writing—review and editing, all authors; visualization, N.M. and H.M.L.; supervision, H.M.L. and M.A.B.P.; project administration, H.M.L.; funding acquisition, H.M.L. and M.A.B.P. All authors have read and agreed to the published version of the manuscript.

Funding: This research received no external funding.

Data Availability Statement: Data will be provided upon request.

Acknowledgments: During the preparation of this manuscript, the authors used ChatGPT 5.6 (OpenAI) for language editing, literature checks, manuscript preparation, and assistance with statistical calculation code. The prompts used for the graphical abstract were: '"Create a graphical abstract illustrating citric acid extraction of pectin from yellow passion fruit peel."; "Show the extracted pectin being evaluated separately in films and sunflower-oil emulsions."; "Highlight the favorable performance at 0.086–0.50% citric acid and poorer performance at 10.0%."'. The authors have reviewed and edited the output and take full responsibility for the content of this publication.

Conflicts of Interest: The authors declare no conflicts of interest.

Abbreviations

The following abbreviations are used in this manuscript:

Abbreviation	Definition
ANOVA	Analysis of variance
Ara	Arabinose
ASTM	ASTM International
DE	Apparent titrimetric degree of esterification
D[3,2]	Surface-area-weighted mean droplet diameter
D[4,3]	Volume-weighted mean droplet diameter
EDTA	Ethylenediaminetetraacetic acid
Gal	Galactose
GalA	Galacturonic acid
HG	Homogalacturonan
HPLC	High-performance liquid chromatography
M_v	Apparent viscosity-average molar mass
M_w	Weight-average molar mass
REML	Restricted maximum likelihood
RG-I	Rhamnogalacturonan I
Rha	Rhamnose
SD	Standard deviation
TFA	Trifluoroacetic acid
WVP	Water-vapor permeability
η_0	Cross-estimated zero-shear viscosity
η_{50}	Apparent viscosity at 50 s^{-1}

References

1. Abboud, K.; Iacomini, M.; Simas, F.; Cordeiro, L. High methoxyl pectin from the soluble dietary fiber of passion fruit peel forms weak gel without the requirement of sugar addition. *Carbohydr. Polym.* **2020**, *246*, 116616. [CrossRef] [PubMed]
2. Cui, J.; Zhao, C.; Feng, L.; Han, Y.; Du, H.; Xiao, H.; Zheng, J. Pectins from fruits: Relationships between extraction methods, structural characteristics, and functional properties. *Trends Food Sci. Technol.* **2021**, *110*, 39–54. [CrossRef]
3. Pinheiro, E.R.; Silva, I.M.; Gonzaga, L.V.; Amante, E.R.; Teófilo, R.F.; Ferreira, M.M.; Amboni, R.D. Optimization of extraction of high-ester pectin from passion fruit peel (*Passiflora edulis flavicarpa*) with citric acid by using response surface methodology. *Bioresour. Technol.* **2008**, *99*, 5561–5566. [CrossRef] [PubMed]
4. Yapo, B.M. Biochemical characteristics and gelling capacity of pectin from yellow passion fruit rind as affected by acid extractant nature. *J. Agric. Food Chem.* **2009**, *57*, 1572–1578. [CrossRef] [PubMed]
5. Liang, Y.; Yang, Y.; Zheng, L.; Zheng, X.; Xiao, D.; Wang, S.; Ai, B.; Sheng, Z. Extraction of Pectin from Passion Fruit Peel: Composition, Structural Characterization and Emulsion Stability. *Foods* **2022**, *11*, 3995. [CrossRef] [PubMed]
6. Huo, D.; Dai, J.; Yuan, S.; Cheng, X.; Pan, Y.; Wang, L.; Wang, R. Eco-friendly simultaneous extraction of pectins and phenolics from passion fruit (*Passiflora edulis* Sims) peel: Process optimization, physicochemical properties, and antioxidant activity. *Int. J. Biol. Macromol.* **2023**, *243*, 125229. [CrossRef] [PubMed]
7. Pereira, D.T.V.; Méndez-Albiñana, P.; Mendiola, J.A.; Villamiel, M.; Cifuentes, A.; Martínez, J.; Ibáñez, E. An eco-friendly extraction method to obtain pectin from passion fruit rinds (*Passiflora edulis* sp.) using subcritical water and pressurized natural deep eutectic solvents. *Carbohydr. Polym.* **2024**, *326*, 121578. [CrossRef] [PubMed]
8. Cho, E.-H.; Jung, H.-T.; Lee, B.-H.; Kim, H.-S.; Rhee, J.-K.; Yoo, S.-H. Green process development for apple-peel pectin production by organic acid extraction. *Carbohydr. Polym.* **2019**, *204*, 97–103. [CrossRef] [PubMed]
9. Seixas, F.L.; Fukuda, D.L.; Turbiani, F.R.B.; Garcia, P.S.; Petkowicz, C.L.O.; Jagadevan, S.; Gimenes, M.L. Extraction of pectin from passion fruit peel (*Passiflora edulis* f. *flavicarpa*) by microwave-induced heating. *Food Hydrocoll.* **2014**, *38*, 186–192. [CrossRef]
10. Costa, M.E.; Sarinho, A.M.; Lima, J.; Andrade, R.; Baptista, L.; Almeida, R.D.; Lisboa, H.M. Chemical modification of starch for high-performance bioplastics: A critical review of structure–property relationships and scalable processing. *Carbohydr. Polym.* **2026**, *378*, 124906. [CrossRef] [PubMed]
11. Chandrasekar, C.M.; White, A.; Simon, S.; Hotchkiss, A.; Jackson, M.; Evans, K.; Koirala, P.; Goyal, R.; Sablani, S.; Zhao, W. Citric acid-based microwave and ultrasonic extractions of lemon peel pectin and their effects on the properties of pectin films. *Int. J. Biol. Macromol.* **2026**, *344*, 150367. [CrossRef] [PubMed]
12. Chalapud, M.C.; Salgado-Cruz, M.d.l.P.; Baümler, E.R.; Carelli, A.A.; Morales-Sánchez, E.; Calderón-Domínguez, G.; García-Hernández, A.B. Study of the physical, chemical, and structural properties of low- and high-methoxyl pectin-based film matrices including sunflower waxes. *Membranes* **2023**, *13*, 846. [CrossRef] [PubMed]
13. Roy, S.; Zhang, W.; Biswas, D.; Ramakrishnan, R.; Rhim, J.-W. Grapefruit seed extract-added functional films and coating for active packaging applications: A review. *Molecules* **2023**, *28*, 730. [CrossRef] [PubMed]
14. Alba, K.; Kontogiorgos, V. Pectin at the oil-water interface: Relationship of molecular composition and structure to functionality. *Food Hydrocoll.* **2017**, *68*, 211–218. [CrossRef]
15. Ngouémazong, E.D.; Christiaens, S.; Shpigelman, A.; Van Loey, A.; Hendrickx, M. The emulsifying and emulsion-stabilizing properties of pectin: A review. *Compr. Rev. Food Sci. Food Saf.* **2015**, *14*, 705–718. [CrossRef]
16. Wang, Q.; Sun, X.; Qian, Y.; Feng, Y.; Cao, Y.; Wu, M.; Guan, T.; Yu, H. Enhanced emulsification via pH-dependent complexation: Structural and interfacial engineering of hempseed protein hydrolysates by anionic polysaccharides. *J. Food Eng.* **2026**, *418*, 113125. [CrossRef]
17. Humerez-Flores, J.N.; Verkempinck, S.H.E.; Van Loey, A.M.; Moldenaers, P.; Hendrickx, M.E. Targeted modifications of citrus pectin to improve interfacial properties and the impact on emulsion stability. *Food Hydrocoll.* **2022**, *132*, 107841. [CrossRef]
18. Humerez-Flores, J.N.; Verkempinck, S.H.E.; De Bie, M.; Kyomugasho, C.; Van Loey, A.M.; Moldenaers, P.; Hendrickx, M.E. Understanding the impact of diverse structural properties of homogalacturonan rich citrus pectin-derived compounds on their emulsifying and emulsion stabilizing potential. *Food Hydrocoll.* **2022**, *125*, 107343. [CrossRef]
19. Yu, Y.; Wang, Y.; Liu, X.; Liu, Y.; Ji, L.; Zhou, Y.; Sun, L. Comparison of analytical methods for determining methylesterification and acetylation of pectin. *Appl. Sci.* **2021**, *11*, 4461. [CrossRef]
20. Amorim, T.A.; Carvalho, A.J.d.B.A.; da Silva Figueiredo, L.; dos Santos Lima, M.; Sarinho, A.M.; Santos, N.C.; Lisboa, H.M.; Gusmão, T.A.S.; de Pereira Gusmão, R. Structure-Function Relationship and Antioxidant Mechanisms of Pectin from Red and White Pitaya Peels for Functional Food Applications. *Food Hydrocoll.* **2025**, *167*, 111455. [CrossRef]
21. Cross, M.M. Rheology of non-Newtonian fluids: A new flow equation for pseudoplastic systems. *J. Colloid Sci.* **1965**, *20*, 417–437. [CrossRef]

22. Ribeiro, S.; Nascimento, A.; Lima, J.; Lima, L.; Almeida, R.; Lisboa, H. Modulation of rheological and textural properties in avocado pulp: Impact of maltodextrin concentration and temperature. *Food Mater. Res.* **2024**, *4*, e014. [CrossRef]
23. Martins Duarte, M.E.; Pereira, T.R.R.; Vieira, A.F.; Santos, N.C.; Gouveia, D.S.; Lisboa, H.M.; Rocha, A.P.T. Development and Characterization of Cassava Starch Films Enriched with Cassava Root Cortex Extract: Functional, Structural, and Biodegradability Insights. *J. Packag. Technol. Res.* **2025**, *9*, 125–140. [CrossRef]
24. *ASTM D882*; Standard Test Method for Tensile Properties of Thin Plastic Sheeting. ASTM International: West Conshohocken, PA, USA, 2026.
25. *ASTM E96/E96M*; Standard Test Methods for Gravimetric Determination of Water Vapor Transmission Rate of Materials. ASTM International: West Conshohocken, PA, USA, 2024.
26. Grazi, A.; Nascimento, A.; Almeida, R.; Costa, M.E.; Sousa, S.; Lisboa, H.M. First-principles modeling and optimization of the dip-coating process for starch-glycerol edible films using viscosity measurements. *Colloids Surf. A Physicochem. Eng. Asp.* **2025**, *716*, 136712. [CrossRef]
27. Jiang, H.; Zhang, W.; Khan, M.R.; Ahmad, N.; Rhim, J.-W.; Jiang, W.; Roy, S. Film Properties of Pectin Obtained from Various Fruits' (Lemon, Pomelo, Pitaya) Peels. *J. Compos. Sci.* **2023**, *7*, 366. [CrossRef]
28. Shuai, X.; Chen, J.; Liu, Q.; Dong, H.; Dai, T.; Li, Z.; Liu, C.; Wang, R. The Effects of Pectin Structure on Emulsifying, Rheological, and In Vitro Digestion Properties of Emulsion. *Foods* **2022**, *11*, 3444. [CrossRef] [PubMed]
29. Wandee, Y.; Uttapap, D.; Mischnick, P. Yield and structural composition of pomelo peel pectins extracted under acidic and alkaline conditions. *Food Hydrocoll.* **2019**, *87*, 237–244. [CrossRef]
30. Ma, M.; Cui, J.; Zhang, Y.; Blecker, C.; Zheng, J. Changes in molecular structure of citrus pectin in acidic environments at ambient temperature. *Carbohydr. Polym.* **2025**, *356*, 123411. [CrossRef] [PubMed]
31. Van Audenhove, J.; Bernaerts, T.; De Smet, V.; Delbaere, S.; Van Loey, A.; Hendrickx, M. The Structure and Composition of Extracted Pectin and Residual Cell Wall Material from Processing Tomato: The Role of a Stepwise Approach versus High-Pressure Homogenization-Facilitated Acid Extraction. *Foods* **2021**, *10*, 1064. [CrossRef] [PubMed]
32. Cruz, R.d.C.A.L.; Diniz, L.G.M.; Lisboa, H.M.; Fook, M.V.L. Effect of different carboxylic acids as solvent on chitosan fibers production by wet spinning. *Matéria* **2016**, *21*, 525–531. [CrossRef]
33. Lisboa, H. Reinforcement of poly (vinyl alcohol) films with alpha-chitin nanowhiskers. *Polímeros* **2018**, *28*, 69–75. [CrossRef]
34. Fei, W.; Wu, Z.; Cheng, H.; Xiong, Y.; Chen, W.; Meng, L. Molecular mobility and morphology change of poly(vinyl alcohol) (PVA) film as induced by plasticizer glycerol. *J. Polym. Sci.* **2023**, *61*, 1959–1970. [CrossRef]
35. Chuenkaek, T.; Nakajima, K.; Kobayashi, T. Water-soluble pectin films prepared with extracts from *Citrus maxima* wastes under acidic conditions and their moisturizing characteristics. *Biomass Convers. Biorefinery* **2024**, *14*, 23921–23934. [CrossRef]
36. Mikus, M.; Galus, S. The Effect of Phenolic Acids on the Sorption and Wetting Properties of Apple Pectin-Based Packaging Films. *Molecules* **2025**, *30*, 1960. [CrossRef] [PubMed]
37. Zhang, H.; Fan, Z.; Peng, D.; Huang, C.; Wu, X.; Sun, F. Tunning the hydrophobic performance and thermal stability of pectin film by acetic anhydride esterification. *Int. J. Biol. Macromol.* **2024**, *276*, 133746. [CrossRef] [PubMed]
38. Lima, J.; Morais, Y.D.d.; Fernandes, L.; Andrade, R.; Batista, L.; Sarinho, A.M.; Costa, M.E.; Almeida, R.D.; Lisboa, H.M. Gum Arabic Modification Routes for Food Colloids and Encapsulation: Structure–Property–Process Relationships and Engineering Trade-Offs. *Colloids Interfaces* **2026**, *10*, 37. [CrossRef]
39. Baldino, N.; Mileti, O.; Gabriele, D. Rheological surface properties of commercial citrus pectins at different pH and concentration. *LWT* **2018**, *93*, 124–130. [CrossRef]
40. Alba, K.; Kontogiorgos, V. Emulsification properties of pectin. In *Pectin: Technological and Physiological Properties*; Springer: Cham, Switzerland, 2020; pp. 83–97.
41. Hua, X.; Liu, J.; Guan, S.; Tan, J.; Wang, M.; Yang, R. Surface activity of ultrahigh methoxylated pectin of different size. *Food Hydrocoll.* **2021**, *113*, 106495. [CrossRef]
42. Gawkowska, D.; Cieśla, J.; Zdunek, A.; Cybulska, J. Cross-linking of diluted alkali-soluble pectin from apple (*Malus domestica* fruit) in different acid-base conditions. *Food Hydrocoll.* **2019**, *92*, 285–292. [CrossRef]
43. Niu, H.; Chen, X.; Luo, T.; Chen, H.; Fu, X. Relationships between the behavior of three different sources of pectin at the oil-water interface and the stability of the emulsion. *Food Hydrocoll.* **2022**, *128*, 107566. [CrossRef]
44. Sarinho, A.M.; Andrade, R.; Lima, J.; Batista, L.; Nascimento, A.; Almeida, R.; Lisboa, H.M. Exploiting xanthan–guar gum interactions for stable avocado oil emulsions: A multi-stage kinetic and rheological approach. *J. Food Eng.* **2026**, *403*, 112741. [CrossRef]
45. Schroën, K.; de Ruiter, J.; Berton-Carabin, C. The Importance of Interfacial Tension in Emulsification: Connecting Scaling Relations Used in Large Scale Preparation with Microfluidic Measurement Methods. *ChemEngineering* **2020**, *4*, 63. [CrossRef]

46. Touma, K.; Lebaz, N.; Sheibat-Othman, N. Centrifugal creaming of concentrated oil-in-water emulsions: Experimental investigation and modelling. *Chem. Eng. Res. Des.* **2024**, *208*, 899–909. [CrossRef]
47. Song, Y.; Shen, X.; Zhou, G.; Xu, X.; Cao, Y.; Li, W.; Hu, Y.; Zhao, J.; Wu, D.-T.; Huang, Z.; et al. Fabrication and Mechanism of Pickering Emulsions Stability over a Broad pH Range Using Tartary Buckwheat Protein–Sodium Alginate Composite Particles. *Foods* **2025**, *14*, 3429. [CrossRef] [PubMed]

Disclaimer/Publisher's Note: The statements, opinions and data contained in all publications are solely those of the individual author(s) and contributor(s) and not of MDPI and/or the editor(s). MDPI and/or the editor(s) disclaim responsibility for any injury to people or property resulting from any ideas, methods, instructions or products referred to in the content.